Design and experiment of a vegetable plug seedling planting mechanism combining non-circular gear system and multi-link

Lei Wang[1,2], Zhiwen Lin[1], Zhihan Zhou[1], Gaohong Yu[1,2], Zeyu Yang[1], Xuefu Yu[3], Bingliang Ye[1,2*]

(1. *Faculty of Mechanical Engineering, Zhejiang Sci-Tech University, Hangzhou 310018, China*;
2. *Provincial Key Laboratory of Agricultural Intelligent Sensing and Robotics, Zhejiang Province, Hangzhou 310018, China*;
3. *Zhejiang Changshan Mingrui Electromechanical Co., Ltd, Quzhou 324200, China*)

Abstract: To meet the requirements of low damage and high seedling-standing of vegetable plug seedlings during mechanical transplanting, a new seedling planting mechanism combining non-circular gear system and multi-link was developed, which consisted of a five-bar seedling pushing mechanism with the planetary gear train of non-circular gears and a cam linkage seedling supporting mechanism. Based on the agronomic requirements for transplanting vegetable plug seedlings, the design requirements and the poses of four key points of the seedling pushing mechanism were determined. The mechanism solution region synthesis method was applied to conduct precise four poses synthesis of the five-bar seedling pushing mechanism. Based on four key pose points and five additional positions of the seedling pushing trajectory, the angular variation curve of the connecting rod relative to the planetary carrier was derived through cubic B-spline curve fitting. Subsequently, the kinematics analysis of the seedling pushing mechanism was performed to complete continuous motion discrimination and determine the parameters of the five-bar seedling pushing mechanism. The kinematics model of the planetary gear train with non-circular gears was established, and the pitch curve design for each gear was undertaken to fulfill the design of the seedling pushing mechanism. According to the motion law of the seedling pushing mechanism and the seedling planting requirements, the kinematics model of the seedling supporting mechanism was established and its parameters were solved. The virtual simulation analysis and prototype experiment of the mechanism confirm that the simulation and test motion trajectory and key poses are basically consistent with the theoretical design results. Moreover, when the rotation speeds of the seedling planting mechanism are 60-80 r/min, the success rates of broccoli and pepper seedling planting all reach over 93%, indicating the correctness of the seedling planting mechanism design and its application feasibility and universality.

Keywords: vegetable plug seedling transplanter, seedling planting mechanism, solution region synthesis, planetary non-circular gear train, five-bar mechanism

DOI: 10.25165/j.ijabe.20251803.9229

Citation: Wang L, Lin Z W, Zhou Z H, Yu G H, Yang Z Y, Yu X F, et al. Design and experiment of a vegetable plug seedling planting mechanism combining non-circular gear system and multi-link. Int J Agric & Biol Eng, 2025; 18(3): 124–134.

1 Introduction

In recent years, as the largest vegetable producer in the world, China has had approximately 20 million hectares of vegetable planting area each year, accounting for about 50% of global vegetable production. China's vegetable cultivation industry is highly valued due to its position as a pillar industry and a livelihood industry[1,2]. Vegetable plug seedling transplanting, the main mode of vegetable cultivation, offers advantages such as improving land use efficiency, shortening production cycles, and enhancing rooting and seedling strength[3]. However, due to the complexity of China's landforms and the diversity of vegetable varieties, there is still a lack of suitable machines for transplanting vegetable plug seedlings in China, and the mechanization level of vegetable transplanting still needs to be improved[4,5]. Consequently, the innovative design of vegetable plug seedling transplanters has become a prominent research focus in the Chinese vegetable industry.

As the final execution component of the vegetable plug seedling transplanting machine, the seedling planting mechanism directly affects the damage rate and seedling-standing rate of vegetable plug seedlings[6]. Based on the formation of seedling furrow or hole, there are currently two main types of seedling planting mechanisms. The first type is the seedling planting mechanism that uses furrow openers to form seedling furrows, such as chain clip type, flexible disc type, and seedling-guiding tube type[7,8]. The second type is the seedling planting mechanism that uses duckbill planter to prick holes, such as multi-bar type and non-circular gear planetary gear train type[9,10]. These mechanisms still face challenges during transplanting seedlings at high speed. The first type, initially used in semi-automatic transplanting machines, has relatively low transplanting efficiency. Additionally, the chain clip and flexible disc planting mechanisms may damage plug seedlings during seedling clamping, and variation in the positions of the clamped seedlings, as well as the moving speed of transplanting machines, can affect the seedling-standing rate[11-13]. The seedling guiding tube planting mechanism may also affect the seedling-standing rate due to difficulties in controlling the seedling posture while they fall into the seedling furrow[14,15]. The second type of seedling planting mechanism is also difficult to control the trajectory and posture of the planting device during high-speed

Received date: 2024-07-17 **Accepted date:** 2025-02-19

Biographies: Lei Wang, PhD, Lecturer, research interest: intelligent agricultural equipment, Email: leiwang@zstu.edu.cn; **Zhiwen Lin**, MS candidate, research interest: intelligent agricultural equipment, Email: 1780964879@qq.com; **Zhihan Zhou**, MS candidate, research interest: intelligent agricultural equipment, Email: 2557130157@qq.com; **Gaohong Yu**, PhD, Professor, research interests: intelligent agricultural equipment, Email: yugh@zstu.edu.cn; **Zeyu Yang**, MS, research interest: intelligent agricultural equipment, Email: 1559353109@qq.com

***Corresponding author: Bingliang Ye**, PhD, Professor, research interest: intelligent agricultural equipment. Faculty of Mechanical Engineering & Automation, Zhejiang Sci-Tech University, Hangzhou 310018, China. Tel: +86-13336060776, Email: zist_ybl@zstu.edu.cn.

transplanting operations, and the planting device will carry seedlings when it is unearthed, which affects the seedling-standing rate[16].

To address these issues, this paper proposes a new seedling planting mechanism combining non-circular gear system and multi-link, which includes a five-bar seedling pushing mechanism with the planetary non-circular gear train and a cam linkage seedling supporting mechanism. The motion synthesis of the five-bar pushing seedling mechanism was conducted based on four precise poses, and the design of the supporting seedling mechanism cooperating with the seedling pushing mechanism was carried out. The virtual simulation and prototype test were conducted to verify the correctness of the design of the seedling planting mechanism, as well as the working performance.

2 Working principle of seedling planting mechanism

The seedling planting mechanism combining planetary gear train of non-circular gears and multi-link shown in Figure 1 is mainly composed of a five-bar seedling pushing mechanism with planetary non-circular gear train, a cam linkage seedling supporting mechanism, a furrower opener, a seedling guiding tube, etc. The sun gear of the non-circular gear planetary gear train is fixedly connected to the frame and meshed with the first intermediate non-circular gear. The second intermediate non-circular gear is meshed with the planetary non-circular gear. The cam linkage seedling supporting mechanism is a combination mechanism of a swinging follower disc cam mechanism and a rocker slider mechanism.

When the seedling planting mechanism shown in Figure 1 is at work, the planetary carrier 6 of the seedling pushing mechanism rotates clockwise at a constant speed. The seedling pushing plate 11 is driven by the five-bar mechanism coupled with the planetary non-circular gear train to move in the opposite direction of the furrow opener 9, and the vegetable plug seedling 15 in the furrow opener is pushed out to the soil, so the seedling planting operation completes. Simultaneously, the cam linkage seedling supporting mechanism driven by the chain drives to make seedling supporting plate 14 reciprocate in the vertical direction, and cooperates with the seedling pushing mechanism to complete operations of seedling receiving and pushing.

The working process of the seedling planting mechanism includes the two main stages of seedling receiving and seedling pushing. In the seedling receiving stage, the seedling receiving plate of the seedling pushing mechanism and the seedling supporting plate of the seedling supporting mechanism form a wedge-shaped space, and the plug seedling falls into the wedge-shaped space through the seedling guiding tube (as shown in Figure 2a). Then the seedling receiving plate swings back in the forward direction of the furrow opener, allowing the seedlings to slide on the seedling receiving plate and fall to the bottom of the furrow opener. This wedge-shaped seedling receiving method is useful for controlling the falling height of the seedling and reducing seedling damage[17]. After the plug seedling is received, the process transits to the seedling pushing stage. The seedling pushing plate *EP* shown in Figure 2b begins to move to the left to contact the seedlings (shown in Figure 2c). To ensure the uprightness of the plug seedlings, the seedling pushing plate always maintains contact with the seedling, controlling the posture of the seedling until it is pushed out of the furrow opener. At this time, the seedling pushing plate almost moves to the left limit position, while the seedling supporting plate rises to the highest position, ensuring that the seedlings can be smoothly pushed down to the seedling furrow (shown in Figure 2a). Simultaneously, the seedling receiving plate and seedling supporting plate form a wedge-shaped space for receiving seedling again (shown in Figure 2a). After the seedling is pushed into the furrow, the covering wheels located behind the furrow opener cover and compact the soil around the seedling, completing one seedling planting operation. After the seedling pushing stage, the seedling planting mechanism returns to its initial position to prepare for the next seedling transplanting cycle.

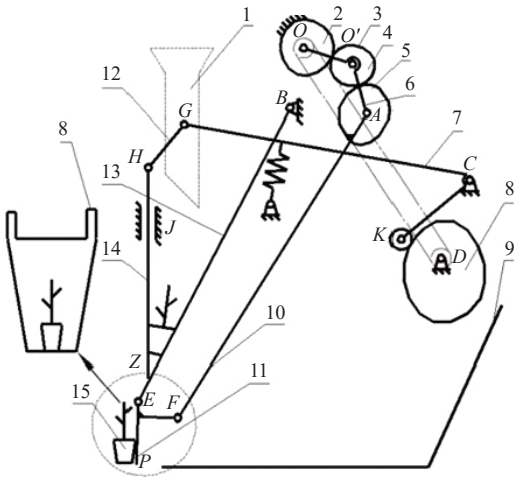

1. Seedling guiding tube 2. Sun gear 3. First intermediate non-circular gear 4. Second intermediate non-circular gear 5. Non-circular planetary gear 6. Planetary carrier 7. Swing rod 8. Cam 9. Furrow opener 10. Connecting rod I 11. Seedling pushing plate 12. Connecting rod II 13. Seedling receiving plate 14. Seedling supporting plate 15. Plug seedling

Figure 1 Diagram of seedling planting mechanism combining planetary gear train of non-circular gears and multi-link

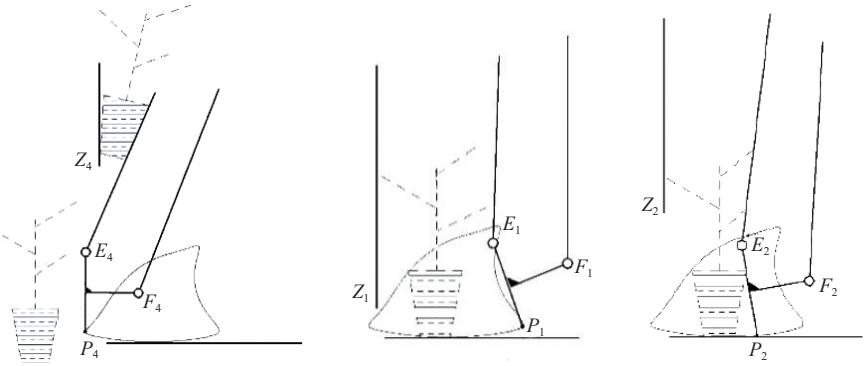

a. Seedling receiving moment

b. Start moment of seedling pushing

c. Contact moment of seedling pushing plate with seedling

Figure 2 Diagram of working process of seedling planting mechanism

3 Design of five-bar seedling pushing mechanism with planetary non-circular gear train

3.1 Design requirements and key pose points of seedling pushing mechanism

As shown in Figures 1 and 2, the motion characteristics of the seedling pushing plate, such as the motion trajectory and posture of the five-bar seedling pushing mechanism with planetary non-circular gear train, directly affect the planting effect of vegetable plug seedlings. Therefore, to ensure reliable seedling planting and meet the requirements for high uprightness and low damage of seedlings, the key pose points must satisfy the following design objectives:

1) P_1 is the right extreme pose point of the motion trajectory of point P of the seedling pushing plate and serves as the reference benchmark for other key pose points. To ensure the stable movement of the seedlings during the seedling pushing process, the horizontal displacement of point P of the seedling pushing plate should be greater than the width of the stems and leaves of the vegetable seedlings, which is about 110 mm to 130 mm, while its vertical displacement should be as small as possible, between 5 mm and 10 mm. Therefore, the horizontal distance between the remaining key pose points and P1 should not exceed 130 mm, and the vertical distance should not exceed 10 mm.

2) P_2 is the pose point of point P when the seedling pushing plate just contacts with the seedling. To prevent the seedling plug from tipping over upon contact, the seedling pushing angle between the seedling pushing plate and negative direction of x-axis should be 80° to 90°.

3) P_3 is the pose point of point P when the plug seedling is pushed into the furrow. To ensure that the plug seedlings enter the seedling furrow as vertically as possible, the angle range of the seedling pushing plate should be set between 88° and 92°.

4) P_4 is the left extreme pose point of the motion trajectory of point P of the seedling pushing plate. To ensure a smooth transition during the return motion, P_4 is required to move no more than 40 mm to the left relative to P_3, with the seedling pushing plate angle variation maintained between 88° and 95°, achieving deceleration and preventing excessive inertial force during the return process.

The relevant data for the four key pose points of the five-bar seedling pushing mechanism are listed in Table 1.

Table 1 Data of four key pose points of five-bar seedling pushing mechanism

Pose points	Horizontal coordinate x_i/mm	Vertical coordinate y_i/mm	Seedling pushing angle θ_i/(°)
P_1	–23.1	–309.7	66.2
P_2	–51.1	–314.6	80.0
P_3	–104.5	–314.8	90.0
P_4	–138.9	–309.0	90.8

3.2 Synthesis of five-bar seedling pushing mechanism

Without considering the planetary gear train, the five-bar seedling pushing mechanism with the planetary gear train can be simplified as a closed-chain five-bar mechanism composed of 2R and 3R open-chain. Therefore, this paper applies the solution region method to synthesize the five-bar seedling pushing mechanism. Based on the poses of points P_1-P_4 in the end of the seedling pushing plate of the seedling pushing mechanism in Section 2.1, the motion synthesis of the open-chain 2R and 3R mechanisms are conducted, respectively, and the feasible solution region for the five-bar mechanism is constructed. Then according to the four key pose points and five additional positions of the seedling pushing trajectory, the angular variation curve of the connecting rod relative to the planetary carrier is derived through cubic B-spline curve fitting. Finally, the kinematics analysis of the seedling pushing mechanism is carried out to discriminate the continuity of the mechanism, and then the parameters of the five-bar seedling pushing mechanism are determined, and the pitch curve design of non-circular gears of the planetary gear train is fulfilled.

3.2.1 Solution region construction of five-bar seedling pushing mechanism

In this paper, the Burmester curve equations are applied to derive the solution curve of the five-bar seedling pushing mechanism. The Burmester curve method enables the synthesis of three to five precise poses to generate all mechanism solutions that meet the pose constraints[18]. By translating algebraic problems into geometry, the solution is visualized using curves, such as the center point curve and the dot curve, to help design and visualize[19]. As shown in Figure 3, the planes where the rods Bb and Mm are located are π_1 and π_2, respectively. The initial positions are π_1^1 and π_2^1, and the positions in the ith position are π_1^i and π_2^i. The azimuth angle of the straight lines b_iL_{bi} and m_iL_{mi} are α_i and β_i, respectively. The hinge points B and M are located in the planes π_1 and π_2, respectively, and their coordinates at the four positions are $B_i=(x_{Bi}, y_{Bi})$, $M_i=(x_{Mi}, y_{Mi})$.

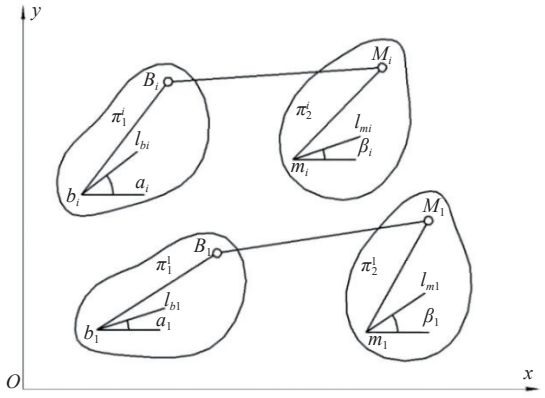

Figure 3 Motion analysis diagram of rigid body plane

According to the constant distance between pivots B and M, the following equation is established:

$$[B_i - M_i]^{\mathrm{T}}[B_i - M_i] = [B_1 - M_1]^{\mathrm{T}}[B_1 - M_1],\ i = 2,3,4 \quad (1)$$

By the conditions of the solution of Equation (1), the binary cubic equation satisfied by the coordinates x_{M1} and y_{M1} of hinge point M is obtained.

$$H_1\left(x_{M1}^3 + x_{M1}y_{M1}^2\right) + H_2\left(y_{M1}^3 + y_{M1}x_{M1}^2\right) + H_3x_{M1}^2 + H_4y_{M1}^2 + H_5x_{M1}y_{M1} + H_6x_{M1} + H_7y_{M1} + H_8 = 0 \quad (2)$$

The coordinate solution set of hinge point M in motion position 1 can be obtained after the data of the four poses P_1-P_4 in Section 2.1 are substituted into Equation (2). The coordinates of hinge point B in the corresponding motion position 1 can also be calculated out after one of these solutions is substituted into Equation (1).

Since the 3R mechanism with four poses is constrained by an incomplete dataset in motion synthesis, relevant unknown parameters must be given for constraints[20]. In this paper, the coordinates of the fixed hinge point O are given as (0, 0), and the phase differences of the planetary carrier OA at each known position relative to the initial position are 18°, 50°, and 90°, respectively. The length ranges of the constrained rods EP and FP

and the range of horizontal coordinates of hinge points E and F are listed in Table 2.

Computer-aided analysis and design software for the five-bar seedling pushing mechanism with the planetary gear train was developed based on MATLAB. After the data of the determined four pose positions and related constraint parameters are input in the main interface of the software shown in Figure 4, the Burmester curves, the feasible solution region of the mechanism, transmission ratio curve, pitch curves of non-circular gears, and seedling pushing trajectory can be obtained through the mechanism motion synthesis.

Table 2 Limit range of relevant rods length and hinge point coordinates

Parameter	*EP* length/mm	*FP* length/mm	Horizontal coordinate x_E of point E	Horizontal coordinate x_F of point F
Parameter ranges	[55,100]	[20,100]	[–100,0]	[–20,50]

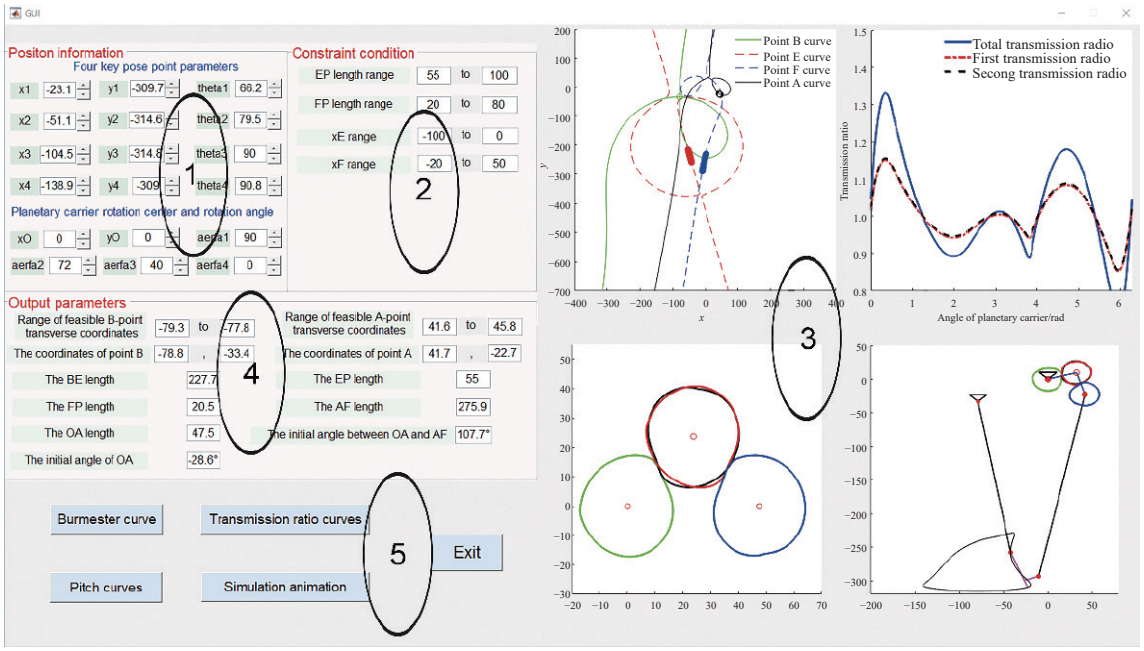

Figure 4 Computer-aided analysis and design software for five-bar seedling pushing mechanism

After the solution curves of the five-bar seedling pushing mechanism are obtained through the software, the motion defects of open-chain 2R and 3R mechanisms are discriminated[21], and solutions of the mechanisms with motion defects are eliminated. The solution regions of the open-chain 2R and 3R mechanisms are obtained, respectively. The parameters of the 2R and 3R mechanisms in the solution regions are combined to construct planar five-bar mechanisms for selecting the feasible solutions of the five-bar mechanism by taking the existence condition of crank as the constraint[22]. The feasible solution regions of hinge points of the five-bar seedling pushing mechanism, namely the bolded parts of the hinge point solution curves, are obtained and shown in Figure 5.

3.2.2 Parameter solution of five-bar seedling pushing mechanism

All possible mechanisms are selected sequentially in the solution region of the closed-chain five-bar mechanism, and the planetary gear train with non-circular gears replaces the side link to transfer the five-bar mechanism with double degrees of freedom to the gear-connecting rod combination mechanism with one degree of freedom to meet the design requirements. The rotation angles of the rods at these moments are determined based on the above four key pose positions of the seedling pushing plate. However, since the continuous motion of the five-bar mechanism cannot be determined with only four poses, five additional positions during the return stage of the mechanism are added. Then the cubic B-spline curve is used to fit the cycle rotation angle curve of connecting rod Ⅰ relative to the planetary carrier, by which the motion analysis of the five-bar mechanism is carried out to determine the mechanism solutions meeting the periodic continuous motion. Finally, the non-circular gear pitch curves of planetary gear train are designed based on the mechanism solutions. The technical route is shown in Figure 6.

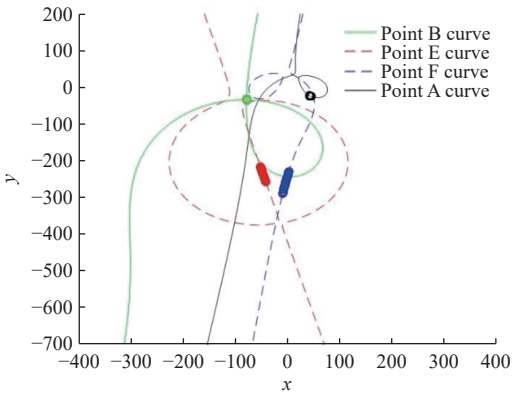

Figure 5 Hinge point solution curves and feasible solution region of five-bar seedling pushing mechanism

In the previous section, four key position points of the five-bar seedling pushing mechanism were provided; however, these points only correspond to the pushing phase, lacking position information for the return phase. As a result, the operational trajectory and the rotation angle of the connecting rod I relative to the planetary carrier could not be fully fitted. Therefore, five additional auxiliary position points are introduced, which should be within the allowable range of the link length to prevent the motion trajectory from being unachievable due to being too large or too small, ensuring the completeness and continuity of the trajectory fitting. The positions

and coordinates of the five additional positions of the seedling pushing plate in the return stage of the mechanism are shown in Figure 7 and Table 3, respectively.

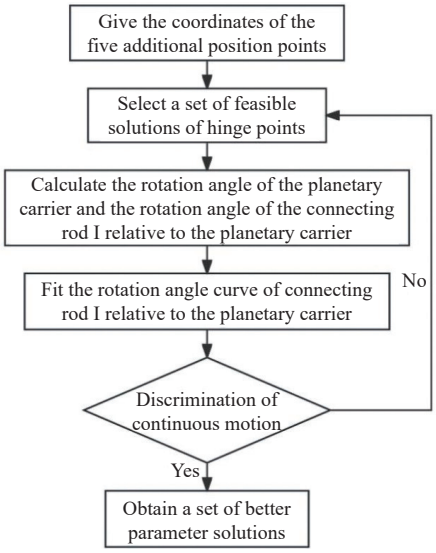

Figure 6 Technical route diagram of parameter solution for five-bar seedling pushing mechanism

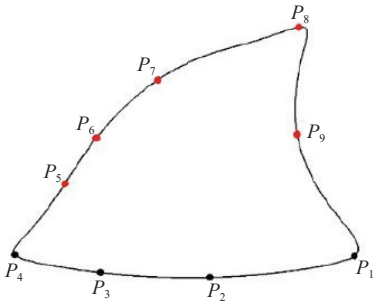

Figure 7 Distribution diagram of trajectory points

Table 3 Coordinates of the five additional positions

Positions	Horizontal coordinate x_i	Vertical coordinate y_i
P_5	–125	–287
P_6	–115	–272
P_7	–85	–244
P_8	–39	–229
P_9	–41	–266

Figure 8 shows the diagram of the five-bar seedling pushing mechanism with planetary gear train, taking the fixed hinge point O as the origin of the rectangular coordinate system. The motion analysis of the seedling pushing mechanism is carried out.

According to the formula for the intersection of two circles, x_E^i and y_E^i, the horizontal and vertical coordinates of point E at position i, can be obtained. According to the geometric relationship, the following coordinates of point F can also be obtained:

$$\begin{cases} x_F^i = \cos\left(\text{atan}\left(\dfrac{x_P^1 - x_E^1}{y_E^1 - y_P^1}\right) + \dfrac{\pi}{2} + \theta_6\right) L_{FP} + x_P^i \\ y_F^i = \sin\left(\text{atan}\left(\dfrac{x_P^1 - x_E^1}{y_E^1 - y_P^1}\right) + \dfrac{\pi}{2} + \theta_6\right) L_{FP} + y_P^i \end{cases} \tag{3}$$

where, (x_F^i, y_F^i), (x_P^1, y_P^1), (x_E^1, y_E^1), and (x_P^i, y_P^i) are the coordinates of point F at position i, point P at position 1, point E at position 1, and point P at position i, respectively. θ_6 is the angle between the seedling pushing plate EF and PE. L_{EP} is the length of the seedling pushing plate EF.

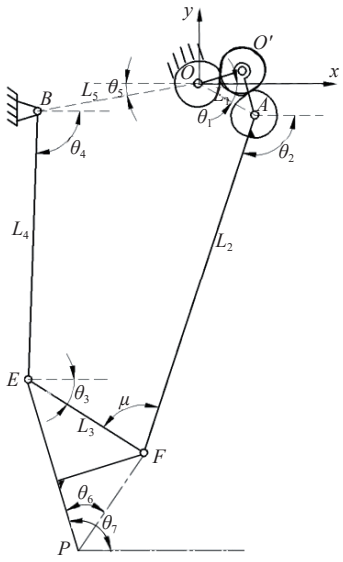

Figure 8 Diagram of five-bar seedling pushing mechanism with planetary gear train

In the same way, according to the formula for the intersection of two circles, x_A^i and y_A^i, the horizontal and vertical coordinates of point A at position i, can be obtained. According to the trigonometric relationship, the rotation angles of the connecting rod Ⅰ and planetary carrier can be obtained.

$$\begin{cases} \theta_1^i = \text{asin}\left(\dfrac{x_A^i}{L_1}\right) \\ \theta_2^i = \text{atan}\left(\dfrac{x_A^i - x_F^i}{y_A^i - y_F^i}\right) - \dfrac{\pi}{2} \end{cases} \tag{4}$$

where, θ_1^i and θ_2^i are the rotation angles of the planetary carrier and connecting rod Ⅰ at position 1. (x_A^i, y_A^i), and (x_F^i, y_F^i) are the coordinates of point A at position i and point F at position i, respectively. L_1 is the length of OA rod.

B-spline curves exhibit high degrees of freedom, where modifying a control point only affects the shape of the curve adjacent to that point. Their favorable mathematical properties enable precise representation of various complex shapes, thus offering superior performance in function fitting[23,24]. Therefore, the following curve equation is used for the cubic B-spline curve fitting of the rotation angle of the connecting rod I relative to the planetary carrier.

$$P(u) = \sum_{i=0}^{n} P_i B_{i,k}(u), \quad u = (u_{k-1}, u_{n+1}) \tag{5}$$

where, P_i is the selected feature point. $B_{i,k}(u)$ is the basis function of order k (k–1), and its formula is as the following:

$$\begin{cases} B_{i,1}(u) = \begin{cases} 1, & u_i < u < u_i \\ 0, & \text{others} \end{cases} \\ P_i B_{i,k}(u) = \dfrac{u - u_i}{u_{i+k-1} - u_i} B_{i,k-1}(u) + \dfrac{u_{i+k} - u}{u_{i+k} - u_{i+1}} B_{i+k,k-1}(u) \end{cases} \tag{6}$$

where, u_i is the node value. U, equal to (u_0, u_1, u_{n+k}), is the node vector, and that 0/0 is equal to 0 is defined.

From the closed vector polygon $OAFEB$, the closed vector equation can be obtained as the following:

$$\overrightarrow{OA} + \overrightarrow{AF} = \overrightarrow{OB} + \overrightarrow{BE} + \overrightarrow{EF} \tag{7}$$

The projection equation is obtained from Equation (7). After elimination of θ_3 and organization of the equation, the following

equation is obtained:

$$\begin{aligned} &L_1^2+L_2^2-L_3^2+L_4^2+L_5^2+2L_1L_5\cos(\theta_1+\theta_5)+\\ &2L_2L_5\cos(\theta_2+\theta_5)-2L_4L_5\cos(\theta_4+\theta_5)+\\ &2L_1L_2\cos(\theta_1-\theta_2)-2L_1L_4\cos(\theta_1-\theta_4)-\\ &2L_2L_4\cos(\theta_2-\theta_4)=0 \end{aligned} \tag{8}$$

where, L_2, L_3, and L_4 are the length of connecting rod Ⅰ, rod EF, and seedling plate BE, respectively. θ_1, θ_2, θ_3, and θ_4 are the angles between rod OA, connecting rod Ⅰ, rod EF, and seedling plate BE and positive direction of x-axis, respectively. θ_5 is the angle between BO and negative direction of x-axis. Letting x_4 be equal to tan (θ_5/2), Equation (8) can be simplified and organized as the following:

$$A_1x_4^2+B_1x_4+C_1=0 \tag{9}$$

where,

$$\begin{aligned} A_1=&L_1^2+L_2^2-L_3^2+L_4^2+L_5^2+2L_1L_5\cos(\theta_1+\theta_5)-2L_1L_4\cos\theta_1+\\ &2L_4L_5\cos\theta_5+2L_1L_2\cos(\theta_1-\theta_2)+2L_2L_5\cos(\theta_2+\theta_5)-\\ &2L_2L_4\cos\theta_2;\\ B_1=&-4L_4L_5\sin\theta_5+4L_1L_4\sin\theta_1+4L_2L_4\sin\theta_2;\\ C_1=&L_1^2+L_2^2-L_3^2+L_4^2+L_5^2+2L_1L_5\cos(\theta_1+\theta_5)+2L_1L_2\cos(\theta_1-\theta_2)+\\ &2L_2L_5\cos(\theta_2+\theta_5)-2L_4L_5\cos\theta_5-2L_1L_4\cos\theta_1-2L_2L_4\cos\theta_2; \end{aligned}$$

Equation (9) is a univariate quadratic equation. When A_1 is not equal to zero, the continuous motion condition of the five-bar seedling pushing mechanism with planetary gear train of non-circular gears is obtained as the following equation:

$$\Delta=B_1^2-4A_1C_1\geq 0 \tag{10}$$

After kinematics synthesis of the five-bar seedling pushing mechanism completes, a set of feasible solutions is selected from suitable solutions region of the mechanism, and kinematics analysis of the five-bar seedling pushing mechanism with non-circular gear planetary gear train after the rotation angle fitting is carried out. If the continuous motion condition as Equation (10) is not satisfied, a feasible solution is reselected for fitting and discrimination. Finally, the functional relationship between the rotation angles θ_2 and θ_1 of the connecting rod and planetary carrier is obtained, as well as a set of optimal parameters meeting the continuous motion condition of the five-bar mechanism[25], as shown in Figure 9 and Table 4, respectively. As shown in Figure 9, the relative angular relationship exhibits a variable transmission ratio, which cannot be effectively addressed by traditional gears. In contrast, non-circular gears combine the advantages of cams and circular gears, enabling precise realization of the variable transmission ratio, making them more suitable for this application[26].

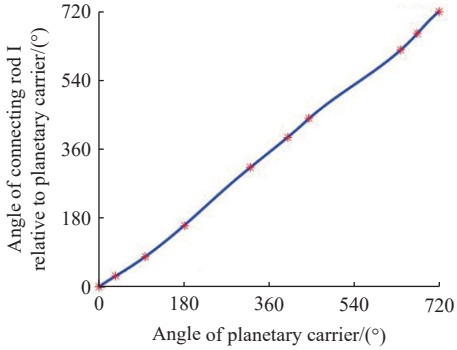

Figure 9 Rotation angle fitting curve of connecting rod I relative to planetary carrier

Table 4 Main parameters of five-bar seedling pushing mechanism

Parameter	Value
Length of planetary carrier/mm	47.47
Length of connecting rod I/mm	275.88
Length of seedling push plate/mm	55.01
Length of seedling receiving plate/mm	227.68
Coordinate of frame hinge point B	(–78.83, –33.37)
Angle of planetary carrier at position 1/(°)	–28.59
Angle of connecting rod I at position 1/(°)	–100.88

3.3 Design of planetary non-circular gear train

The total transmission ratio i_0 of the planetary non-circular gear train is equal to the reciprocal of the slope of rotation angle curve of the connecting rod Ⅰ relative to the planetary carrier. The use of a two-stage gear transmission can effectively reduce the mass and volume of the planetary gear train, making the transmission more compact[27]. To ensure that the non-circular gears exhibit favorable kinematic performance, the distributed stage transmission ratios should have similar amplitudes. Therefore, the square root of the total transmission ratio is taken to obtain the uncorrected first-stage transmission ratio:

$$\begin{cases} i_0=\dfrac{-d\theta_1}{d(\theta_1-\theta_2)} \\ I_1=\sqrt{i_0} \end{cases} \tag{11}$$

where, i_0 is the total transmission ratio of non-circular gear train, andI_1 is the transmission ratio of the uncorrected first-stage gear drives.

However, the pair of non-circular gears generated using the uncorrected transmission ratio may result in unequal pitch curve lengths, failing to meet the requirement for the driving and driven gears to complete one full rotation during engagement. Therefore, a correction factor k is introduced for adjustment, and the corrected first- and second-stage non-circular gear transmission ratios are:

$$\begin{cases} k=\dfrac{2\pi}{\int_0^{2\pi}\dfrac{1}{I_1}d(\theta_1-\theta_2)} \\ \bar{I}_1=\dfrac{I_1}{k} \\ \bar{I}_2=\dfrac{i_0}{\bar{I}_1} \end{cases} \tag{12}$$

where, k is the adjustment coefficient for peak and valley values; $\bar{I}_1$ and $\bar{I}_2$ are the transmission ratios of the corrected first- and second-stage gear drives, respectively.

Based on the gear meshing characteristics[28], the pitch curve equations of the sun gear and first intermediate gear are obtained as the following:

$$\begin{cases} r_1(\varphi_1)=\dfrac{a}{1+\bar{I}_1} \\ r_2(\varphi_2)=a-r_1(\varphi_1) \\ \varphi_2=\int_0^{\varphi_1}\bar{I}_1d\varphi_1 \end{cases} \tag{13}$$

where, $r_1(\varphi_1)$ is the radial diameter of the pitch curve of the non-circular sun gear; φ_1 is the angular displacement of the sun gear; $r_2(\varphi_2)$ is the radial diameter of the pitch curve of the first intermediate non-circular gear; a is the length of the planetary carrier; φ_2 is the angular displacement of the first intermediate non-circular gear. Similarly, the pitch curve equations of the planetary non-circular gear and second intermediate gear can be obtained.

According to the above solution method of the total transmission ratio curve of the planetary non-circular gear train, total transmission ratio assignment, and the pitch curves of non-circular gears[26], the results are shown in Figures 10a and 10b.

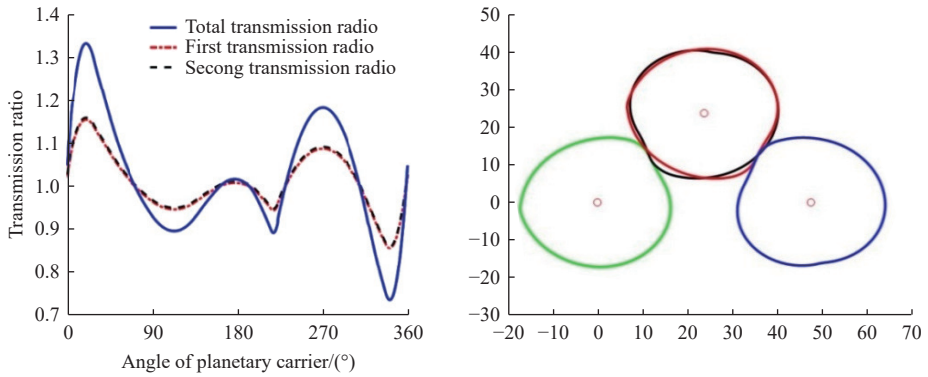

a. Transmission ratio curves of planetary non-circular gear train

b. Pitch curves of non-circular gears

Figure 10 Transmission ratio curves and pitch curves of planetary gear train with non-circular gear

4 Design of cam linkage seedling supporting mechanism

As shown in Figure 11, the cam linkage seedling supporting mechanism drives the seedling supporting plate *HZ* to reciprocate up and down, cooperating with the seedling pushing mechanism to complete the seedling receiving and pushing operations. Therefore, based on the motion law of the seedling pushing mechanism, the design requirements for the seedling supporting mechanism are proposed as follows:

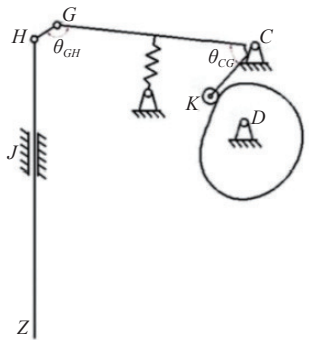

Figure 11 Diagram of seedling supporting mechanism

(1) To effectively prevent the seedling dumping and improve the seedling uprightness degree, it is necessary to minimize the height of point *Z* of the seedling supporting plate but not to collide with the furrower opener while the plug seedling falls inside the furrower opener, as shown in Figure 2b.

(2) To ensure the smooth seedling pushing out of the furrower opener, it is necessary to ensure that the position of point *Z* of the seedling supporting plate is higher than the height of the seedlings at the moment of pushing out the seedling, as shown in Figure 2c.

(3) To reduce the damage rate of the seedlings, it is necessary to ensure that the wedge-shaped space is formed between the seedling receiving plate and seedling supporting plate for seedling receiving while the seedling is pushed out of the furrower opener, as shown in Figure 2a.

The seedling supporting mechanism in Figure 11 utilizes the same coordinate system as Figure 8. According to the motion law of the seedling pushing plate in the seedling pushing mechanism, the coordinates (x_Z, y_{Zi}) and (x_C, y_C) of point *Z* of the seedling supporting plate and the rotation center point *C* of the oscillating bar are determined, then the coordinates of point *G* and point *H* can be obtained.

$$\begin{cases} x_G = x_C + l_{CG}\cos\theta_{CGi} \\ y_G = y_C + l_{CG}\sin\theta_{CGi} \\ x_H = x_G + l_{GH}\cos\theta_{GHi} = x_Z \\ y_H = y_G + l_{GH}\sin\theta_{GHi} = y_{Zi} + l_{HZ} \end{cases} \tag{14}$$

where, θ_{CGi} is angle between *CG* section of oscillating bar and positive direction of *x*-axis; l_{CG} is length of *CG* section of the oscillating bar; l_{GH} is length of the connecting rod II; θ_{GH} is angle between *CG* section of the oscillating bar and positive direction of *x*-axis; l_{HZ} is length of the seedling supporting plate *HZ*.

Subsequently, the coordinates (x_Z, y_{Z1}) and (x_Z, y_{Z2}) of point *Z* at the start moment and end moment of seedling pushing are given, then the maximum angular displacement ψ of the oscillating bar *CG* can be obtained.

$$\psi = \theta_{CG1} - \theta_{CG2} \tag{15}$$

The horizontal displacement curve of the hinge point *E* of the seedling receiving plate is shown in Figure 12. To prevent interference between the seedling supporting plate and the seedling receiving plate, the horizontal coordinate of the supporting plate should be smaller than the minimum value of the horizontal displacement curve at point *E*. Therefore, the horizontal coordinate of the seedling supporting plate is given as –130.

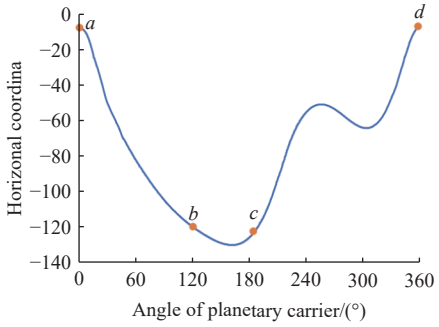

Figure 12 Horizontal displacement curve of hinge point *E* of seedling receiving plate

To prevent interference between the seedling receiving plate and the opener, the lowest position of the seedling receiving plate is set to 5 mm above the furrow opener. Additionally, to prevent interference between the seedling receiving plate and the plug seedling, the highest position of the seedling supporting plate

should exceed the height of the plug seedling (124 mm). By substituting the two sets of extreme position information (–130, 5) and (–130, 124) into Equations (14) and (15), the main parameters of the seedling supporting mechanism are listed in Table 5.

Table 5 Parameters of seedling supporting mechanism

Parameter	Value	Parameter	Value
l_{HZ}/mm	116	x_C	65.40
l_{GH}/mm	30	y_C	–80.00
l_{CG}/mm	200	x_D	143.86
l_{CK}/mm	58	y_D	42.03
$\angle KCG$	30°	ψ	36°

From stage *a* to stage *b*, which is the pushing phase, the seedling supporting plate should move from its lowest position to the highest position. This process corresponds to the cam's pushing stroke, with the cam rotation angle of 110°. From stage *b* to stage *c*, which is the receiving phase, the seedling supporting plate should remain stationary at the highest position, while the seedling receiving plate and the seedling supporting plate form a wedge-shaped structure to receive the seedlings. This process corresponds to the cam's far rest position phase, with the cam rotation angle of 80°. From stage *c* to stage *d*, which is the return phase, the seedling supporting plate should move from the highest point to the lowest point and remain stationary at the lowest point for a period of time. This process corresponds to the cam's return stroke and near rest position phases, with the cam return angle of 85° and the near rest angle of 85°. According to the angular change of the cam at each stage, the oscillation law of the cam follower applies simple harmonic motion. Given that the cam base circle radius is 30 mm and the roller radius is 6 mm, the theoretical contour curve and actual contour curve of the cam shown in Figure 13 can be determined. The displacement curve of the seedling support plate shown in Figure 14 is obtained according to the designed cam mechanism.

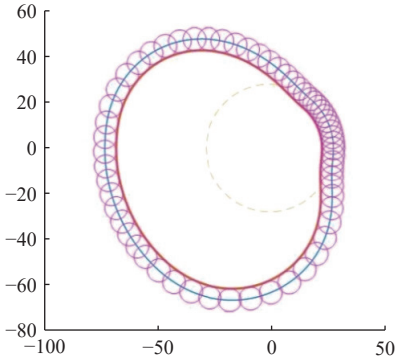

Figure 13 Cam contour curve

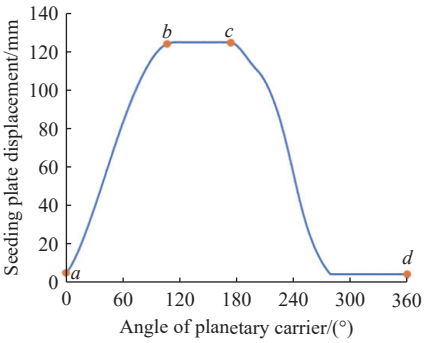

Figure 14 Displacement curve of seedling supporting plate

5 Simulation analysis and prototype tests of seedling planting mechanism

5.1 Simulation analysis of seedling planting mechanism

The structural design of the seedling planting mechanism combining non-circular gear system and multi-link was carried out according to the optimized parameters of the mechanism. The assembled 3D model was imported into Adams software to conduct virtual simulation. The simulation trajectory curves and key poses of the seedling pushing mechanism shown in Figure 15 are basically consistent with theoretical results, respectively, and the seedling supporting mechanism can cooperate well with the seedling pushing mechanism, which verifies the correctness of the mechanism design.

5.2 Prototype tests of seedling planting mechanism

To master the actual kinematic characteristics of the designed seedling planting mechanism and verify its seedling planting effect, the physical prototype of the seedling planting mechanism and seedling planting test bench shown in Figure 16 were developed for conducting idle test and the seedling planting tests of the mechanism. The test bench consists of the hauling equipment and seedling planting mechanism.

5.2.1 Prototype idle test

The purpose of the prototype idle test is to obtain the actual motion trajectory and key poses of the mechanism to master its kinematic characteristics and further compare whether the trajectory and poses of the mechanism prototype are consistent with the theoretical results. The manufactured and assembled prototype was installed on the test bench, and the motion processes of the seedling planting mechanism were photographed using the high-speed camera. The actual motion trajectory formed by the seedling pushing plate and the poses at the moments of the seedling receiving and planting were measured and obtained, as shown in Figure 17.

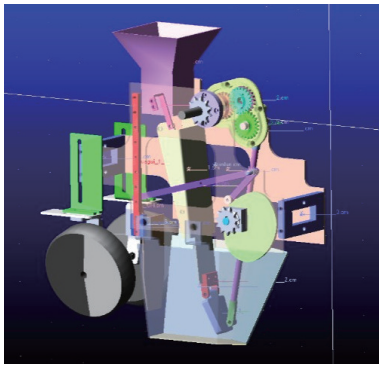

a. Model of seedling planting mechanism

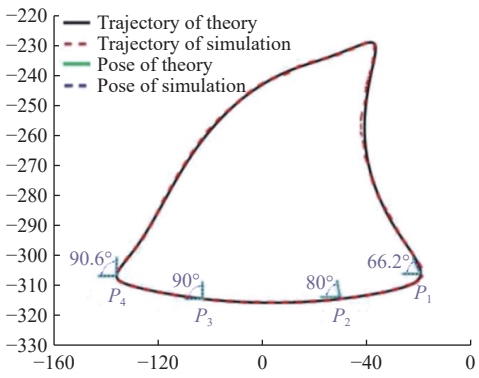

b. Comparison of trajectory and poses of seedling pushing plate

Figure 15 Virtual simulation of seedling planting mechanism

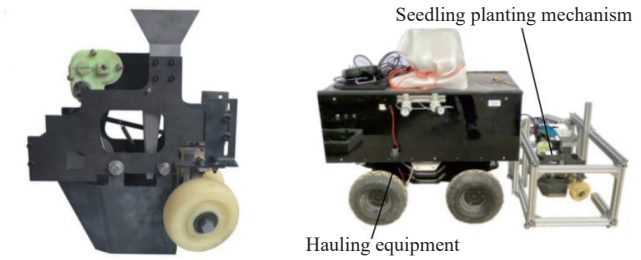

a. Prototype of seedling planting mechanism b. Test bench for seedling planting

Figure 16 Prototype and test bench of seedling planting mechanism

Through comparing the test trajectory of the mechanism shown in Figure 17 with the theory and simulation trajectories, it can be concluded that they are basically consistent. The test posture angles of the seedling pushing plate were compared with the theoretical results, as can be seen in Table 6. It can be found that the errors between the test and theoretical seedling pushing angle are all less than 2°, which satisfy the allowable error of the mechanism. Therefore, by comparing and analyzing the trajectory and seedling pushing angle of the prototype with those of simulation and theory, it can be concluded that the kinematic characteristics of the prototype of the seedling planting mechanism meet the seedling planting requirements, which further verifies the correctness of the mechanism design method and results.

5.2.2 Prototype seedling planting test

To further verify the seedling effect and application feasibility of the seedling planting mechanism, the seedling planting test bench was constructed for seedling planting tests. As shown in Figure 18a, the test soil ridge with length, width, and height of 6 m, 0.4 m, and 0.08 m was constructed in the laboratory. In addition, in order to show the universality of the seedling planting mechanism for vegetable plug seedlings, broccoli and pepper seedlings of 128 hole trays with an age of 30 d were taken as the experimental seedlings, as shown in Figures 18b and 18c, respectively.

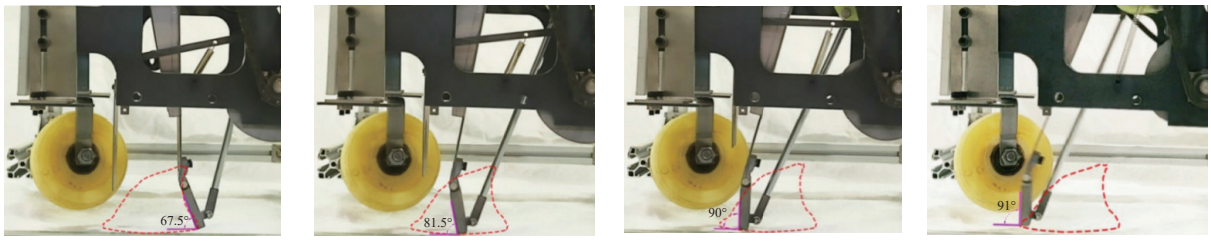

a. Seedling pushing angle at position 1 b. Seedling pushing angle at position 2 c. Seedling pushing angle at position 3 d. Seedling pushing angle at position 4

Figure 17 Test trajectory and key poses of seedling pushing mechanism

Table 6 Seedling pushing angles comparison between results of test and theory

Positions	Seedling pushing angle of theory/(°)	Seedling pushing angle of test/(°)	Error/(°)
Position 1	66.2	67.5	1.3
Position 2	80.0	81.5	1.5
Position 3	90.0	90.0	0
Position 4	90.8	91.0	0.2

a. Indoor soil ridge b. Broccoli seedling c. Pepper seedling

Figure 18 Test conditions for seedling planting

The planting quality of plug seedlings is assessed according to the agricultural industry standard NY/T 1924-2010, which applies to the transplanting of plug seedlings for most vegetables. The quality of transplanting is determined by the depth and uprightness of the plug seedlings. These are key indicators for determining whether the planting quality meets the requirements. The planting depth is defined as the vertical distance from the upper surface of the plug to the soil surface. When this distance is greater than 0.9 times and less than 1.5 times the height of the plug, the planting depth is considered qualified, as shown in Figure 19. The uprightness refers to the angle between the main stem of the seedling and the horizontal plane. If the angle is greater than 45°, the uprightness is deemed qualified, as shown in Figure 20. If both the planting depth and uprightness of the seedling meet the standard, the planting of the seedling is considered qualified.

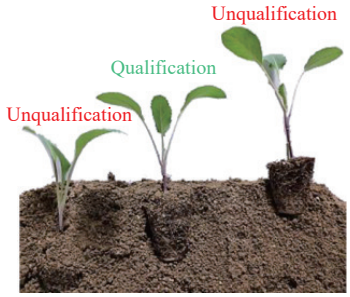

Figure 19 Plug seedling planting depth standard

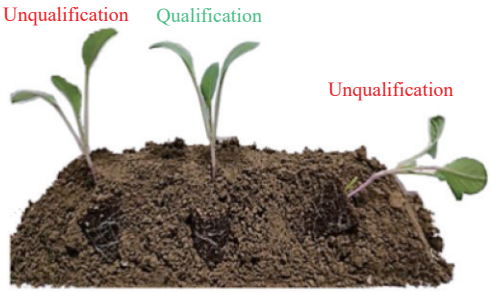

Figure 20 Plug seedling planting uprightness standard

According to the seedling bowl height of about 36 mm, and with soil piles about 10 mm in height on both sides of the seedling groove after the furrow opener completes furrow operation, the ditch depth is selected as 40 mm, and the actual depth of the seedling groove is 50 mm. In the seedling planting tests, a total of

384 vegetable plug seedlings were used, consisting of 192 broccoli seedlings and 192 pepper seedlings. Six independent transplanting tests were conducted for these two types of seedlings. Three groups of seedling planting tests were conducted for each kind of seedling under the rotation speeds 60 r/min, 70 r/min, and 80 r/min of the mechanism, respectively, with 64 plug seedlings in each group. The seedling planting effect is shown in Figure 21. During each group of seedling planting tests, the number of plug seedlings unsuccessfully planted was recorded, and finally the success rates of seedling planting tests were calculated out, as listed in Table 7.

a. Planting effect of broccoli seedlings b. Planting effect of pepper seedlings c. The planting depth effect of vegetableplug seedlings d. The planting uprightness effect of plug seedling

Figure 21 Seedling planting effect of vegetable plug seedlings

Table 7 Results of seedling planting tests

Seedling species	Rotation speed/ r·min^{-1}	Total number of seedlings	Number of seedlings unsuccessfully planted	Success rate/%
Broccoli seedling	60	64	1	98.4
	70	64	2	96.9
	80	64	3	95.3
Pepper seedling	60	64	2	96.9
	70	64	2	96.9
	80	64	4	93.8

Through the seedling planting tests, it can be found that the success rate of seedling planting slightly decreases with the increase of mechanism rotation speed. At the same time, when rotation speeds of the seedling planting mechanism are 60 r/min to 80 r/min, the planting success rates of the two kinds of vegetable plug seedlings reach more than 93%, and while rotation speed is not higher than 70 r/min, the success rates reach more than 95%, which verifies the application feasibility and universality of the designed seedling planting mechanism combining non-circular gear train and multi-link.

6 Conclusions

According to the transplanting requirements of low damage rate and high seedling-standing rate for vegetable plug seedlings, a new seedling planting mechanism combining non-circular gear system and multi-link was designed in the paper. The virtual simulation analysis, kinematics, and seedling planting tests of the mechanism were conducted. The following conclusions can be drawn:

(1) The mechanism solution region synthesis method was applied to conduct precise four poses synthesis of the five-bar seedling pushing mechanism with planetary non-circular gear train. Furthermore, the seedling supporting mechanism cooperating with the seedling pushing mechanism was designed. The results of the mechanism virtual simulation show that the design of the seedling planting mechanism is correct, and the designed seedling planting mechanism can employ the wedge-shaped seedling receiving method to reduce the damage of plug seedlings, and it can ensure smooth seedling pushing, thereby achieving a high seedling-standing rate.

(2) The kinematic test results of the seedling planting mechanism show that the designed mechanism can meet the transplanting requirements of kinematics trajectory and key poses for vegetable plug seedling. Further, through seedling planting tests taking broccoli and pepper plug seedlings as test objects, it was found that the planting success rates of the two kinds of vegetable plug seedlings reach more than 93% when the rotation speeds of the seedling planting mechanism are 60-80 r/min. While the rotation speed is not higher than 70 r/min, the success rates reach more than 95%, which verifies the application feasibility and universality of the designed seedling planting mechanism. The mechanism exhibits a high transplantation success rate, effectively preserving the integrity of the seedling substrate during transplantation, thereby promoting healthy crop growth. The application of this technology is expected to significantly increase crop yield while ensuring its stability, providing a positive contribution to the modernization and sustainable development of agriculture.

Acknowledgements

This study was financially supported by the National Natural Science Foundation of China (Grant No. 32171899) and Zhejiang Provincial Natural Science Foundation of China (Grant No. LD24E050007).

[References]

[1] Zhang X Y, Bao J, Xu S W. Vegetable monitoring and early warning technology system innovative development for the future. Vegetables, 2023; 7(1): 1–9. (in Chinese).

[2] Zhang J, Liu J F, Zhou X Y, Wu J Z, Shen C. Vegetable market analysis in 2022 and outlook for 2023. China Vegetables, 2023; 1(1): 1–6.

[3] Liao P, Meng Y, Chen Y Q, Weng W A, Chen L, Xing Z P, et al. Potted-seedling machine transplantation simultaneously promotes rice yield, grain quality, and lodging resistance in China: a meta-analysis. Agronomy, 2022; 12(12): 3003.

[4] Wen Y S, Zhang J X, Tian J Y, Duan D S, Zhang Y, Tan Y Z, et al. Design of a traction double-row fully automatic transplanter for vegetable plug seedlings. Computers and Electronics in Agriculture, 2021; 182(1): 106017.

[5] Zhou M L, Shan Y Y, Xue X L, Yin D Q. Theoretical analysis and development of a mechanism with punching device for transplanting potted vegetable seedlings. Int J Agric & Biol Eng, 2020; 13(4): 85–92.

[6] Jin X, Cheng Q, Zhao B, Ji J T, Li M Y. Design and test of 2ZYM-2 potted vegetable seedlings transplanting machine. Int J Agric & Biol Eng, 2020; 13(1): 101–110.

[7] Yan W, Hu M J, Li K, Wang J, Zhang W Y. Design and experiment of horizontal transplanter for sweet potato seedlings. Agriculture, 2022; 12(5): 6775.

[8] Ji J T, Cheng Q, Jin X, Zhang Z H, Xie X L, Li M Y. Design and test of 2ZLX-2 transplanting machine for oil peony. Int J Agric & Biol Eng, 2020; 13(4): 61–69.

[9] Sun L, Xu H C, Zhou Y Z, Shen J H, Yu G H, Hu H F, et al. Kinematic synthesis and simulation of a vegetable pot seedling transplanting mechanism with four exact task poses. Int J Agric & Biol Eng, 2023; 16(2): 85–95.

[10] Yu G H, Wang L, Sun L, Zhao X, Ye B L. Advancement of mechanized transplanting technology and equipments for field crops. Transactions of the CSAM, 2022; 53(9): 1–20.

[11] Wu G W, An X F, Yan B G, Li L W, He Y F. Design and experiment of automatic transplanter for sweet potato naked seedlings based on pretreatment seedling belt. Transactions of the CSAM, 2022; 53(S1): 99–109.

[12] Zhang J Q, Niu Z R, Li T H, Wu Y Q, Xi R, Li Y H, et al. Design and optimization of planting process parameters for 2ZYX-2 type green onion ditching and transplanting machine. Phyton, 2020; 89(1): 147–166.

[13] He Y F, Zhu Q Z, Fu W Q, Luo C H, Cong Y, et al. Design and experiment of a control system for sweet potato seedling-feeding and planting device based on a pre-treatment seedling belt Journal of Agricultural Engineering, 2022; 53(3): 1261. Doi: 10.4081/jae.2022.1261.

[14] Zhang Z, Igathinathane C, Flores P, Ampatzidis Y, Liu H, Mathew J, et al. Time effect after initial wheat lodging on plot lodging ratio detection using UAV imagery and deep learning. In: Zhang Z, Liu H, Yang C, et al. (eds), Unmanned Aerial Systems in Precision Agriculture. Smart Agriculture, Vol 2, Springer, Singapore, 2022; pp.59–72. Doi: 10.1007/978-981-19-2027-1_4.

[15] Javidan S M, Mohammadzamani D. Design, construction and evaluation of semi-automatic vegetable transplanter with conical distributor cup. SN Applied Sciences, 2019; 1(9): 999.

[16] Chen J N, Huang Q Z, Wang Y, Zhang G F. Kinematics modeling and analysis of transplanting mechanism with planetary elliptic gears for pot seedling transplanter. Transactions of the CSAE, 2012; 28(5); 6-12. (in Chinese)

[17] Yang W, Tang T, Yu G H, Du C C, Ye B L. Study on mechanism and test of low damage seedling grafting in pot of the ditch seedling planting mechanism. Journal of Chinese Agricultural Mechanization, 2023; 28(5): 9–15.

[18] Chen C, Bai S, Angeles J. A comprehensive solution of the classic Burmester problem. Transactions of the Canadian Society for Mechanical Engineering, 2008; 32(2): 137–154.

[19] Bourrelle J, Chen C, Caro S, Angeles J. Graphical user interface to solve the burmester problem. IFToMM World Congress, 2007; pp.1–8. Doi: 10.1201/b15883-9.

[20] Bai S P. Dimensional synthesis of six-bar linkages with incomplete data set. New Trends in Mechanism and Machine Science, Springer International Publishing, 2014; pp.3–11. Doi: 10.1007/978-3-319-09411-3_1.

[21] Wang J, Ting K L, Xue C. Discriminant method for the mobility identification of single degree-of-freedom double-loop linkages. Mechanism and Machine Theory, 2010; 45(5): 740–755.

[22] Nie L Y, Ding H F, Wang J, Bi S S. Branch graph method for crank judgement of complex multi-loop linkage. Journal of Beijing University of Aeronautics and Astronautics, 2022; 48(10): 1863–1874.

[23] Gálvez A, Iglesias A. Firefly algorithm for explicit B-spline curve fitting to data points. Mathematical Problems in Engineering, 2013; 2013(1): 528215.

[24] Dung V T, Tjahjowidodo T. A direct method to solve optimal knots of B-spline curves: An application for non-uniform B-spline curves fitting. PloS one, 2017; 12(3): e0173857.

[25] Ma J, Lu A E, Chen C, Ma X D, Ma Q C. Full rotatability and singularity of six-bar and geared five-bar linkages. Journal of Mechanisms & Robotics: Transactions of the ASME, 2010; 2(1): 011011. Doi: 10.1115/1.4000517.

[26] Liu D W, Ren Y T. Creating pitch curve of closed noncircular gear by compensation method. Journal of Mechanical Engineering, 2011; 47(13): 147–152.

[27] Wang L, Fang Z C, Wang Z T, Sun L, Yu G H, Cui R J. Mixed multi pose synthesis method and applications of unequal velocity planetary gear. China Mechanical Engineering, 2024; 35(12): 2211–2220.

[28] Ye J, Zhao X, Wang Y, Sun X C. A novel planar motion generaten method based on the synthesis of planetary gear train with noncircular gears. Journal of Mechanical Science and Technology, 2019; 33: 4939–4949.